ACS OMEGA

Article

Cite This: ACS Omega 2018, 3, 937−945

Predicting Ligand-Free Cell Attachment on Next-Generation Cellulose−Chitosan Hydrogels

Marcus A. Johns,[†,‡,⋈] Yongho Bae,[∥] Francisco E. G. Guimarães,[⊥] Evandro M. Lanzoni,[#,▽] Carlos A. R. Costa,[#] Paul M. Murray,[○] Christoph Deneke,[#,◆] Fernando Galembeck,[#,¶] Janet L. Scott,[*,‡,§] and Ram I. Sharma[*,†,‡]

[†]Department of Chemical Engineering, [‡]Centre for Sustainable Chemical Technologies, and [§]Department of Chemistry, University of Bath, Bath BA2 7AY, U.K.

[∥]Department of Pathology and Anatomical Sciences, Jacobs School of Medicine and Biomedical Sciences, University at Buffalo, The State University of New York, Buffalo, New York 14203, United States

[⊥]Physics Institute of São Carlos, University of São Paulo, São Carlos, SP 13566-590, Brazil

[#]Brazilian Nanotechnology National Laboratory (LNNano), Brazilian Center for Research in Energy and Materials (CNPEM), Campinas, SP 13083-970, Brazil

[▽]Institute of Science and Technology, São Paulo State University (UNESP), Sorocaba, SP 18087-180, Brazil

[○]Paul Murray Catalysis Consulting Ltd., 67 Hudson Close, Yate BS37 4NP, U.K.

[◆]Departamento de Física Aplicada, Instituto de Física "Gleb Wataghin", Universidade Estadual de Campinas − UNICAMP, Campinas, SP 13083-859, Brazil

Supporting Information

ABSTRACT: There is a growing appreciation that engineered biointerfaces can regulate cell behaviors, or functions. Most systems aim to mimic the cell-friendly extracellular matrix environment and incorporate protein ligands; however, the understanding of how a ligand-free system can achieve this is limited. Cell scaffold materials comprised of interfused chitosan−cellulose hydrogels promote cell attachment in ligand-free systems, and we demonstrate the role of cellulose molecular weight, MW, and chitosan content and MW in controlling material properties and thus regulating cell attachment. Semi-interpenetrating network (SIPN) gels, generated from cellulose/ionic liquid/cosolvent solutions, using chitosan solutions as phase inversion solvents, were stable and obviated the need for chemical coupling. Interface properties, including surface zeta-potential, dielectric constant, surface roughness, and shear modulus, were modified by varying the chitosan degree of polymerization and solution concentration, as well as the source of cellulose, creating a family of cellulose−chitosan SIPN materials. These features, in turn, affect cell attachment onto the hydrogels and the utility of this ligand-free approach is extended by forecasting cell attachment using regression modeling to isolate the effects of individual parameters in an initially complex system. We demonstrate that increasing the charge density, and/or shear modulus, of the hydrogel results in increased cell attachment.

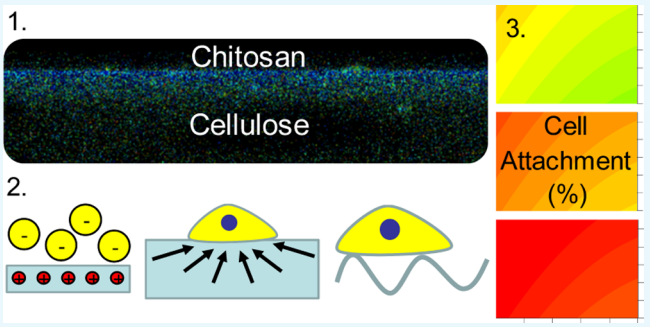

INTRODUCTION

The development of cell scaffolds that successfully mimic the extracellular matrix, ECM, is paramount if tissue engineering is to prove to be efficacious. However, the bulk mechanical properties of many synthetic polymers, although suitable for osseous tissue, are not suitable for soft tissues, such as muscle or nerve tissues, because the physical properties, such as the tensile strength, are not matched.[1−3] The use of ECM and ECM-derived proteins also have associated problems: scaffolds require well-defined microenvironments in which animal byproducts and contaminants are limited, which is difficult to guarantee with animal-derived scaffold materials, and ECM-based scaffolds are often complex, with poorly defined compositions.[4]

To address these problems, alternative biopolymers that mimic the properties of the ECM have been sought. One area of focus is the use of plant-, algae-, and fungi-derived polysaccharides to mimic the physical and chemical properties of hyaluronan (the only naturally occuring glycosaminoglycan that is not sulfated, or bound to a protein-based core to form a

Received: October 17, 2017
Accepted: January 2, 2018
Published: January 25, 2018

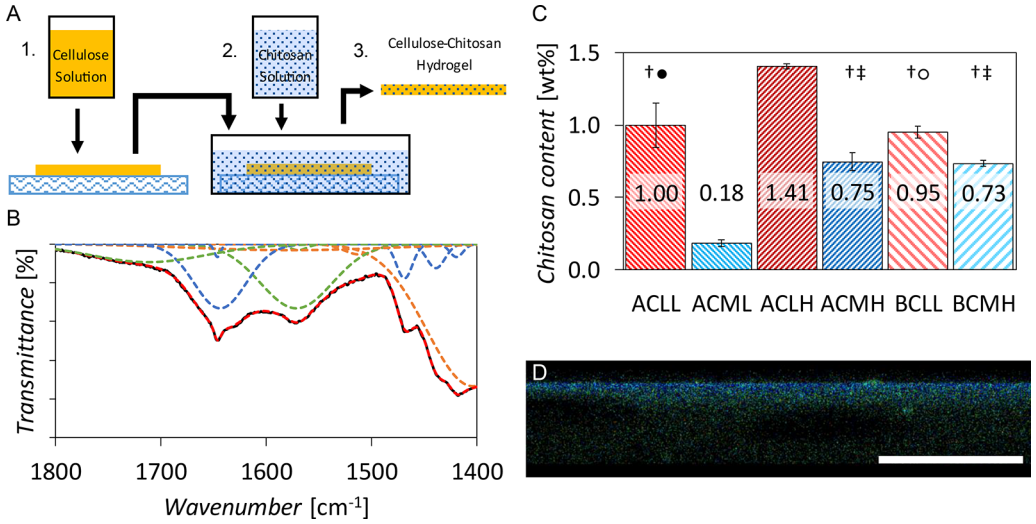

Figure 1. (A) Schematic of SIPN hydrogel generation process. 1. Cellulose is dissolved in an organic electrolyte solution consisting of [EMIm][OAc] and DMSO before being cast on a glass plate. 2. Cellulose film is immersed in a chitosan solution (0.43 M acetic acid, aqueous). 3. After 20 min cellulose−chitosan SIPN hydrogel is removed. (B) Fourier transform infrared (FTIR) of cellulose−chitosan hydrogel demonstrating that both polymers are present. Peaks unique to cellulose in orange; unique to chitosan in green; present in both polymers in blue; summation of fitted peaks in red; raw data in black. (C) Free chitosan content determined by ninhydrin adsorption. Chitosan content is increased by increasing the chitosan solution concentration from 0.12 to 2.1 wt % (xxxL vs xxxH), and decreasing the chitosan molecular weight from 109 to 26 kDa (xxMx vs xxLx). No significant difference is observed between plant α-cellulose, AC, and bacterial α-cellulose, BC, samples. Error ± SE, $N = 3$. † $p < 0.001$ compared to ACML; ‡ $p < 0.001$ compared to ACLH; ○ $p < 0.01$ compared to ACLH; ● $p < 0.05$ compared to ACLH. (D) Confocal image of BCLL demonstrating the presence of chitosan layer (brighter, blue region) at the surface of the cellulose hydrogel (darker, green region). Scale bar 50 μm.

proteoglycan), which is known to be involved in the regulation of cell growth, differentiation, adhesion, and motility.[5] Blends consisting of chitosan and alginate have been generated and reported to result in improved cell response over pure alginate (due to the modified chemical properties) and improved mechanical properties over pure chitosan.[6−8] Alginate, cross-linked with multivalent cations, provides mechanical strength, whereas chitosan imparts appropriate chemical functionality to the material. However, alginate consists of homopolymeric blocks of two epimers in an arrangement that cannot be controlled, and only one of the epimers is involved in cross-linking with the multivalent cations.[9] Therefore, it cannot be guaranteed that the mechanical properties of the scaffold will show batch-to-batch consistency, which could prove challenging at a commercial level. As an alternative to alginate, cellulose has been investigated, with cellulose−chitosan composites generated following codissolution of the polysaccharides in ionic liquids.[10−13] However, discoloration of the composites was reported using the current methodology,[10] indicating the degradation of one of the polymers, or a (currently unidentified) side-reaction.

Successful scaffold design requires an understanding of cell response to the interdependent material properties. It has previously been reported that surface charge,[14−16] tensile strength,[17−20] and surface topography[21−25] affect cell response to a scaffold. Despite this, for the majority of scaffolds reported in the literature, cell response is considered with respect to (i) one variable, ignoring others, or assuming that these are constant;[14,16,20,22] or (ii) two or more variables, but without robust testing of their independence, or determination of individual effects on cell response.[8,15,26] Design of experiments, DoE, based on regression modeling, may be utilized to enable the effect of individual characteristics to be discerned in a complex system, even where responses to changes in individual variables are not independent of each other. However, use of DoE in tissue engineering has been limited and primarily focused on the response of cells to multiligand systems,[27,28] or to elastic modulus and ligand concentration.[29,30]

Here, we report on the generation of cellulose−chitosan scaffolds that enable cell attachment comparable to that on tissue culture plate (polystyrene) (TCP) under ligand-free conditions. We use regression modeling to decouple the effects of scaffold surface charge, surface topography, and mechanical properties on cell attachment. We avoid the reductionist, one variable at a time, approach, which can result in the oversimplification of complex systems, potentially resulting in missed interdependence, thus enabling understanding of the interaction between properties of the surface that, upon cell attachment, becomes the cell/scaffold interface, allowing scaffolds to be designed to maximize cell attachment.

RESULTS AND DISCUSSION

The generation of a cellulose−chitosan hydrogel by phase inversion of cellulose dissolved in an organic electrolyte solution (OES) comprised of 1-ethyl-3-methylimidazolium acetate, [EMIm][OAc], and dimethyl sulfoxide (DMSO) in a chitosan solution (Figure 1A) enables the production of SIPN hydrogels (thickness: 200 μm), without the degradation of either polymer. Two different sources of cellulose, i.e., plant α-cellulose, AC, and bacterial α-cellulose, BC, are tested, as these are known to provide cellulose polymers with a 10-fold difference in the degree of polymerization. Cell attachment (MG-63 cells) comparable to that on TCP is achieved even in the absence of a fetal bovine serum, FBS, usually added to provide complex protein ligands.

To prove the presence of chitosan within the six hydrogels (Table 1) and investigate its penetration, three techniques are employed: Fourier transform infrared (FTIR) spectroscopy,

DOI: 10.1021/acsomega.7b01583
ACS Omega 2018, 3, 937−945

Table 1. Hydrogel Formulations and Their Corresponding Sample Codes

sample	celluose source	chitosan MW (kDa)	chitosan solution concentration (wt %)
AC	plant α-cellulose		
BC	bacterial α-cellulose		
ACLL	plant α-cellulose	26	0.21
ACML	plant α-cellulose	109	0.21
ACLH	plant α-cellulose	26	2.10
ACMH	plant α-cellulose	109	2.10
BCLL	bacterial α-cellulose	26	0.21
BCMH	bacterial α-cellulose	109	2.10
L		26	
M		109	

ninhydrin adsorption, and confocal microscopy. Deconvolution of the FTIR spectrum in the fingerprint region (1400−1800 cm^{-1}) and comparison with the spectra of pure cellulose and chitosan indicates that the hydrogels contain both cellulose and chitosan (Figure 1B). The free chitosan loading is determined via ninhydrin adsorption, and no significant difference is observed between samples prepared from AC or BC (Figure 1C). Confocal microscopy reveals a chitosan-rich region at the surface of the hydrogel, i.e., chitosan is not homogeneously distributed throughout the cast film. For the AC samples, increasing the chitosan solution concentration, and decreasing the chitosan MW, results in an increase in the chitosan penetration (Figure 1D, Table 2). By decreasing the chitosan MW, an increase in chitosan loading and penetration is observed due to the lower MW chitosan being able to access a greater proportion of hydrogel pores, as previously determined using variable-sized biomolecule probes.[31] Differences in the pore structure previously observed between AC and BC hydrogels may account for differences in the chitosan penetration between the two.[31] Although swelling studies are not considered here given that the hydrogels are never dried, a previous study by Liu and Huang suggests that the low chitosan content will not impact the swelling of the hydrogel.[13]

This novel methodology enables the production of SIPN scaffolds, as defined by Alemán et al.[32] The highly dispersed chitosan (the autofluorescent signal of which dominates up to 30% of the scaffold, yet accounts for less than 1.5 wt % of the biopolymer dry material) with a gradated composition (Figure S3) indicates the penetration of chitosan within the previously characterized, highly porous cellulose network.[31] This provides opportunities for use in applications where this would be beneficial, such as membranes that require the material properties of cellulose and the functionality of chitosan. The dissolution of chitosan from the hydrogels upon exposure to acid solutions during ninhydrin adsorption experiments confirms that the polymers are not chemically cross-linked to each other. We therefore expect the hydrogels to be fully biodegradable when exposed to cellulases and chitinases.

As the goal is to fabricate scaffolds that would not require addition of animal-derived proteinaceous ligands, cell attachment in both the presence and absence of FBS is tested. No significant difference is observed between cell attachment in the serum (i.e., protein) positive and negative media for the majority of the hydrogels (Figure 2A). This demonstrates that the cells do not require ligands to mediate the cell−material interface, leading to protein- and serum-free cell attachment. To establish that the cells are binding directly to the hydrogels, pluronic F-127 is used to block nonspecific binding on TCP and selected hydrogels under FBS-negative conditions (Figure 2B). Although a significant decrease is observed on TCP, no significant difference is observed on the cellulose−chitosan hydrogels, confirming that the cells are interacting with the hydrogel surface in a specific manner. Comparison of the hydrogels and TCP under FBS-negative conditions established that ACLL and ACML are not significantly different from TCP whereas ACLH and BCLL are not significantly different from AC (Figure 2C). This indicates that there are differences in the physicochemical cell−material interfacial properties of the hydrogels, affecting cell attachment. Cell morphologies are considered after 24 h in FBS-positive media, and the analysis is included in the Supporting Information (Figures S4−S7).

To determine the cause of differences in cell attachment between the hydrogels, four properties are measured: surface zeta-potential, ζ, which is proportional to the total surface charge; capacitive coupling, dC/dz, which is proportional to the dielectric constant, a measure of polarizability; shear modulus, G, an indicator of the mechanical properties of the hydrogel; and surface root mean square roughness, R_q, an indicator of the surface morphology. The incorporation of chitosan into the hydrogel results in an increase in both ζ (Figure 3A) and dC/dz (Figure 3B) compared to native cellulose, reflecting the pK_a of chitosan (6.2−6.5),[33] which leads to protonation of approximately 10% of the amine groups at pH 7.4. A statistically significant increase in G is observed for ACxL hydrogels (Figure 3C), whereas the xxLx samples are significantly more rough than the other hydrogels (Figure 3D).

Cell attachment on the ACxL hydrogels is not significantly different from TCP (Figure 2C), suggesting that G is critical in determining the extent of cell attachment; G for ACxL hydrogels are significantly different to the other hydrogel samples (Figure 3C). The promotion of cell attachment with an increase in G is in agreement with previous reports.[18,19] However, despite G for ACxH samples being greater than the values for the BCxx samples (Figure 3C), no difference in cell attachment is discerned (Figure 2C). To understand this, other factors are considered: R_q is significantly different for the ACLH and BCLL samples (Figure 3D), suggesting that an increase in R_q negatively impacts cell attachment. The effects of

Table 2. Depth from the Hydrogel Surface to Which Chitosan Autofluorescence (443 nm) is Dominant over Cellulose Autofluorescence (478 nm), As Determined by Confocal Microscopy[a]

sample	ACLL	ACML	ACLH	ACMH	BCLL	BCMH
chitosan depth (μm)	8 ± 2	6 ± 2	28 ± 2	19 ± 2	15 ± 1	10 ± 1

[a]Increased penetration is observed at higher chitosan solution concentrations, and decreased molecular weight. Error ± stack depth.

DOI: 10.1021/acsomega.7b01583
ACS Omega 2018, 3, 937−945

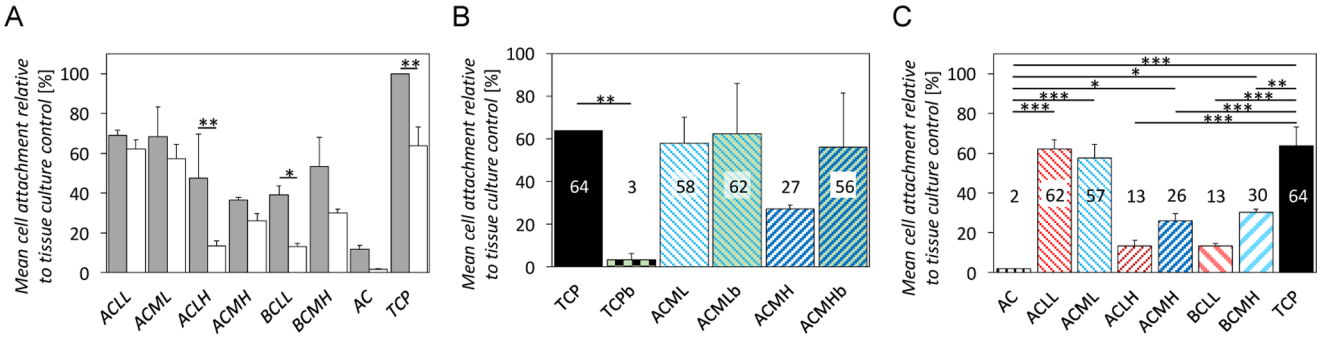

Figure 2. (A) Ninety minute MG63 cell attachment relative to tissue culture plate (TCP) in fetal bovine serum positive (FBS+) media. Attachment was performed in FBS+ (gray bars) and fetal bovine serum negative (FBS−) (white bars) media. No significant difference between FBS+ and FBS− media was observed for most of the cellulose−chitosan hydrogels, indicating that they are suitable for ligand-free cell attachment. Error ± SE, $N = 3$. (B) Comparison of cell attachment with FBS− media on unmodified TCP, ACML, and ACMH, and modified using pluronic F-127 to block nonspecific cell attachment (denoted by "b"). Cell attachment decreases significantly on TCP, but no difference is observed on the hydrogels. Error ± SE, $N = 3$. ** $p < 0.01$. (C) Cell attachment comparison in growth media not containing fetal bovine serum (FBS). No significant difference is observed between TCP and ACLL, or ACML. No significant difference is observed between AC and ACLH, or BCLL. This suggests that there are significant differences in the properties of the hydrogels. Error ± SE, $N = 3$. * $p < 0.05$; ** $p < 0.01$; *** $p < 0.001$.

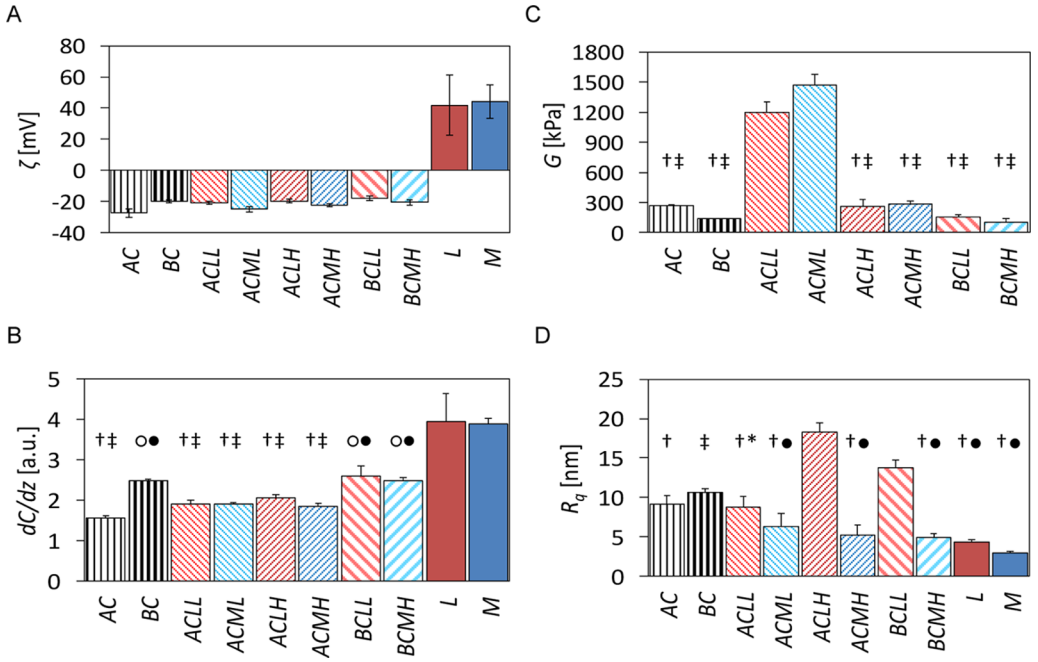

Figure 3. (A) Surface zeta-potential (ζ) of hydrogels. The presence of chitosan results in an increase in ζ compared to pure cellulose. (B) Shear modulus (G) of hydrogels measured via atomic force microscopy (AFM). Generation of AC hydrogels in low chitosan concentration solutions result in a significant increase in G. † $p < 0.001$ compared to ACLL; ‡ $p < 0.001$ compared to ACML. Error ± SE, $N = 4$. (C) Capacitive coupling (dC/dz) of hydrogels measured via electric force microscopy (EFM). The presence of chitosan results in an increase in dC/dz compared to pure cellulose. † $p < 0.001$ compared to low-MW chitosan (L); ○ $p < 0.05$ compared to L; ‡ $p < 0.001$ compared to medium-MW chitosan (M); ● $p < 0.05$ compared to M. Error ± SE; $N \geq 3$. (D) Root mean square roughness (R_q) of hydrogels measured via EFM. Generation of hydrogels in low-MW chitosan concentration solutions result in a significant increase in R_q. † $p < 0.001$ compared to ACLH; ‡ $p < 0.01$ compared to ACLH; ● $p < 0.001$ compared to BCLL; * $p < 0.05$ compared to BCLL. Error ± SE, $N \geq 3$.

ζ and dC/dz on cell attachment are not immediately obvious from direct comparison.

To untangle the effects of each of the individual properties on the resulting cell attachment, multivariate regression modeling, using a "leave-one-out" methodology is employed. All of the possible models containing four- or five-terms are investigated. Interaction terms between two of the properties are included. Average constant values and three coefficients of determination (R^2, Q^2, and MV) are calculated, model validity is determined, and selected models are optimized, as detailed in the Experimental Section.

The four-term model with the additional interaction term ζ^2, and without dC/dz, is determined to be the optimal model to describe cell attachment to the cellulose−chitosan hydrogels under protein-free conditions; $R^2 = 0.88$, $Q^2 = 0.90$, and MV = 0.93 (Figure 4A,B, Table S2). The generation of a three-dimensional contour plot (Figure 4C) enables the effect of each property on cell attachment to be determined. An increase in G promotes the MG63 cell attachment, as previously reported for stromal and hematopoietic cell lines.[18,19] An increase in R_q results in a decrease in cell attachment, in contrast to previous reports, in which the authors suggested that an increase in R_q

DOI: 10.1021/acsomega.7b01583
ACS Omega 2018, 3, 937−945

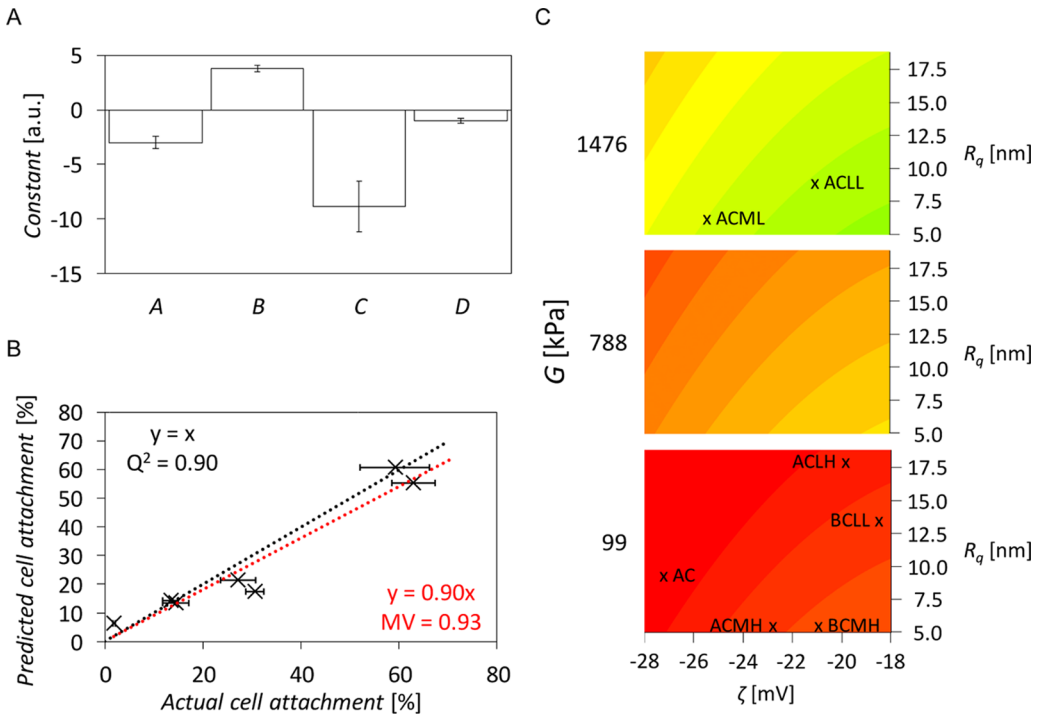

Figure 4. (A) Calculated constants for the four-term regression model, $CA = -3.00\zeta + 0.0379G - 0.889R_q - 0.103\zeta^2$. Normalization: $B \times 10^2$; $C \times 10$; $D \times 10$. Error ± SE, $N = 7$. (B) Predicted vs actual cell attachment for the four-term regression model. Coefficient of determination Q^2 calculated relative to the line $y = x$; MV calculated relative to the line $y = m{\cdot}x$. (C) Three-dimensional contour plot of predicted cell attachment generated using the four-term model. Cell attachment increases as colored bands change from red to green. Relative positions of hydrogels investigated are included. The model suggests that cell attachment increases with increasing ζ and G, which is expected from the literature. Increasing R_q, within the bounds of the system investigated, results in a decrease in cell attachment.

promotes cell attachment.[22,23] Notably, these reports focus on ligand-positive systems, where increasing the hydrophobicity of the material, influenced by the surface topography, increases ligand binding to the scaffold and, therefore, the attachment of cells, which interact directly with the ligands.[34] Indeed, this is observed here with the two scaffolds that are significantly more rough than the others; both ACLH and BCLL show a significant increase in cell attachment in the presence of FBS (Figure 2A). Given the scale over which the roughness changes, it is hypothesized that there is a trade-off between the number of adhesion points that a cell can access (presumed to increase initially with R_q as the surface area will also increase) against the size of the adhesion points between cell and substrate, which are directly proportional to the force that a cell can exert on a substrate.[35] It has previously been demonstrated that the percentage of cells that remain attached after centrifugation increases with initial cell attachment.[22,36] Therefore, as R_q increases, the binding force between the cells and scaffold decreases, resulting in poorer cell attachment.

As ζ increases, the cell attachment also increases. Consideration of the earlier studies on the hydrogels modified using pluronic F-127 (Figure 2B), whereby the blocking of nonspecific binding did not affect the cell attachment to the hydrogels, suggests that the cells are binding directly to the amine groups, which can exhibit a positive charge (as ammonium groups, $-NH_3^+$). Thus, cell attachment appears to be directly proportional to the number of amine groups available at the hydrogel surface.

CONCLUSIONS

To conclude, the regeneration of cellulose hydrogels from organic electrolyte solutions, using a chitosan solution to achieve phase inversion, enabled the generation of robust, semi-interpenetrating network chitosan−cellulose hydrogels without the need for chemical cross-linkers. The presence of the chitosan in the hydrogel scaffold enabled cell attachment in protein-free growth media, with cell attachment to the plant α-cellulose with low concentrations of low molecular weight chitosan hydrogel improved by 3000% compared to pure plant α-cellulose after 90 min. The physicochemical cell−material interfacial properties (surface ζ potential, capacitive coupling, surface roughness, and shear modulus) were modified by varying the cellulose and chitosan degree of polymerization, and chitosan solution concentration (used in phase inversion). This, in turn, affected cell attachment on the hydrogels.

The use of regression modeling enabled the effects of individual parameters to be discerned in an initially complex system, and allowed further development of an understanding of the interaction between cells and their surrounding environment. The developed regression model indicated that an increase in the shear modulus and surface charge, i.e., number of amine groups, and a decrease in the surface roughness were beneficial for MG63 cell attachment within the bounds of the experimental data.

Thus, it is demonstrated that a readily applied procedure for deconvoluting the effect of changes in individual material characteristics on cell attachment allows the importance of specific characteristics to be discerned, thus enabling rational design of these readily fabricated tissue scaffold materials, prepared from natural biopolymers available from nonanimal

DOI: 10.1021/acsomega.7b01583
ACS Omega 2018, 3, 937−945

sources, which promote cell attachment even under ligand-free conditions.

EXPERIMENTAL SECTION

Materials. 1-Ethyl-3-methylimidazolium acetate ([EMIm][OAc]), dimethyl sulfoxide (DMSO), chitosan (low MW and medium MW), plant α-cellulose, acetic acid, glucose, yeast extract, peptone, anhydrous disodium phosphate, citric acid monohydrate, acetate buffer, sodium acetate, ninhydrin, hydrindantin, 2-methoxyethanol, phosphate-buffered saline (PBS), polystyrene latex particles, Dulbecco's modified Eagle's medium (DMEM), fetal bovine serum (FBS), sodium pyruvate, nonessential amino acids (NEAA), penicillin streptomycin (pen strep), formalin, and methanol (MeOH) were purchased from Sigma-Aldrich. Fluorescein phalloidin (FITC), and 4′,6-diamidino-2-phenylindole (DAPI) were purchased from Thermo Fisher Scientific. Plant α-cellulose and [EMIm][OAc] were dried at 60 °C en vacuo overnight; and DMSO dried over activated 4 Å molecular sieves before use.

Bacterial Cellulose Production. Cellulose-producing bacteria from Acetobacter culture were grown in the laboratory at 25 °C in deionized water (DI) supplemented with 2 wt % glucose, 0.5 wt % yeast extract, 0.5 wt % peptone, 0.27 wt % anhydrous disodium phosphate, and 0.15 wt % citric acid monohydrate. The resulting cellulose pellicle was treated with a solution of 10 wt % sodium hypochlorite for 1 h before being washed three times with copious amounts of distilled water and lyophilized.

Hydrogel Generation. Hydrogel codes consisting of four letters (xxxx) were generated based on the choice of cellulose (first two letters); chitosan MW (third letter); and chitosan solution concentration (final letter) as detailed below, and in Table 1.

Cellulose solutions (4 wt %) were prepared in an organic electrolyte solution (OES), consisting of 30:70 (wt %) [EMIm][OAc]/DMSO. For example, for a total of 12.000 g of OES/cellulose solution, 8.064 g DMSO was measured into a vial and 0.480 g α-cellulose (plant, ACxx, or bacterial, BCxx) was added to this and briefly shaken; 3.456 g [EMIm][OAc] was added to the solution, and the mixture agitated on a roller table at ambient temperature overnight, to ensure the complete dissolution of cellulose.

Chitosan solutions (0.12, xxxL, or 2.1 wt %, xxxH; 26, xxLx, or 109 kDa, xxMx) were prepared in 0.43 M acetic acid aqueous solutions.

To generate the hydrogel, cellulose solutions were tape cast using an Elcometer 4340 Automatic Film Applicator with 500 μm between the blade and the glass surface. The resulting film, limited only by the size of the applicator bed, was regenerated by immersion for 20 min in the chosen chitosan solution and washed twice with copious amounts of DI H_2O to remove excess solvent. The resulting hydrogel films were stored in a 20 vol % MeOH aqueous solution to inhibit bacterial growth. For tissue scaffolds based on polysaccharides to be useful, these materials must remain intact in storage. These films proved to be stable throughout the period of experimentation, lasting over one year with no significant differences in cell attachment noted in experiments conducted 12 months apart.

Chitosan Film Generation. Chitosan (2.1 wt %, low, or medium, MW) was dissolved in 0.43 M aqueous acetic acid. These solutions were then poured into a Petri dish and liquid evaporated at 60 °C. The resulting films were washed with DI H_2O before being re-dried.

Fourier Transform Infrared (FTIR) Spectroscopy. FTIR spectra were recorded on a PerkinElmer Frontier FTIR spectrometer in the attenuated total reflection mode between 600 and 4000 cm^{-1} using 10 scans with a resolution of 1 cm^{-1}. The curve-fitting software Fityk was used to deconvolute the raw FTIR data by fitting Gaussian curves to the peaks present in the spectra.[37] Original data are presented in Figure S2.

Chitosan Content Determination. The percentage of free chitosan in the regenerated hydrogels was measured using a method modified from that reported by Tan et al. for determining the chitosan degree of deacetylation using ultraviolet−vis (UV−vis)spectroscopy.[38] Solutions of low- and medium-MW chitosan (1 mg mL^{-1}) were prepared by dissolving the polymer in 0.43 M acetic acid aqueous solution. Calibration solutions (0−200 μg mL^{-1}) were then generated, consisting of 2 mL ninhydrin reagent solution (0.5 mL acetic buffer, 1.5 mL 2-methoxyethanol, 40 mg ninhydrin, 6 mg hydrindantin), 0.5 mL acetic buffer, and 0.5 mL chitosan solution diluted to the required concentration with DI H_2O. The resulting solutions were heated (water bath) at 100 °C for 15 min before being allowed to cool, diluted to 0−20 μg mL^{-1} with DI H_2O, and calibration curves, linking chitosan concentration to UV−vis absorbance at 570 nm, generated using an Agilent Cary 100 UV−vis spectrometer.

To determine the chitosan content in the hydrogels, 20 mg of lyophilized material was added to 20 mL 0.43 M aqueous acetic acid and sonicated (sonication bath, 30 min, 37 Hz, 50 °C). Experimental solutions (2 mL ninhydrin reagent solution, 0.5 mL acetic buffer, 0.5 mL hydrogel solution) were diluted 10-fold and UV−vis absorbance measured in triplicate. The chitosan concentration was determined from the calibration curve, enabling the chitosan weight percentage in the hydrogel to be ascertained.

Confocal Microscopy. Pöhlker et al. reported that cellulose and chitosan autofluoresced with different emission wavelength maxima at 420 and 410 nm under excitation at 335 nm.[39] Based on this, 32-emission channel hydrogel z-stack fluorescence spectra were taken using a Zeiss LSM 780 confocal microscope. Images were obtained using a 405 nm diode laser with a Plan-Apochromat 20×/0.28 M27 objective. An MBS-405 filter was used for the invisible light detector. The maximum distance between slices was 3.6 μm, with a minimum of 20 slices recorded. Hydrogel samples were placed between a glass slide and coverslip to ensure a flat surface. Comparison of the intensity at 443 and 478 nm was used to determine whether chitosan or cellulose was dominant for each slice, enabling the determination of the thickness of the chitosan dominant region at the surface of the hydrogel (Table 2, Figure S3).

Surface ζ Potential. The ζ of the hydrogels were established using a Malvern Zetasizer Surface ζ Potential Cell. An aqueous suspension of polystyrene latex particles (diameter: 0.3 μm) in PBS (pH 7.4) was used as the tracer solution. Five measurements, consisting of 15 repeats each, were performed for each distance for each hydrogel.

Atomic Force Microscopy. Shear moduli were determined by AFM as previously described by Bae et al.[40,41] Hydrogels were placed in a 35 mm plastic dish, immobilized with vacuum grease, and submerged in 3 mL PBS. A DAFM-2X BioScope AFM system (Bruker) in force mode was applied to measure the shear modulus of the hydrogels. The hydrogels were indented with a silicon nitride cantilever (spring constant: 0.06 N m^{-1}) with a conical tip (40 nm in diameter); 8 to 10 measurements of each hydrogel were collected and analyzed

DOI: 10.1021/acsomega.7b01583
ACS Omega 2018, 3, 937−945

per condition. To calculate the shear modulus, the first 600 nm of tip deflection from the horizontal was fitted with the Hertz model for a cone.[42] The data were analyzed using custom-built MATLAB scripts.

Scanning Probe Microscopy. Hydrogel samples were flash frozen and dried using a mini lyotrap freeze dryer (LTE Scientific). Topography, phase contrast, electric potential, and capacitive coupling, dC/dz, images of the dried hydrogels were obtained using a NX-10 Atomic Force Microscope (Park System) in an intermittent contact mode.[43] PPP-EFM probes (NanoWorld) were used for measurements (spring constant: 2.8 N m^{-1}, resonance frequency: 75 kHz). Hydrogel samples were fixed onto metal sample stubs using a double-sided adhesive tape and topography and electrical images acquired in air by a single-pass scanning (ambient temperature, humidity 0−5%). Analysis and processing of the AFM images were carried out with Gwyddion.[44] The hydrogel dC/dz signal distribution was calculated from LockIn3 Amplitude data file using the one-dimensional height analysis function, and the surface roughness from the flattened height data file using the roughness parameter function.

Cell Attachment. Hydrogel samples were prepared from the generated sheets using a 10 mm hole punch, generating circles that fitted snugly into 48-well tissue culture treated plates (Costar). The samples were washed twice under sterile conditions with PBS before being stored in 1 mL PBS overnight at 4 °C. For the nonspecific blocking studies, 0.5 mL 0.5 wt % pluronic F-127 in PBS was preadsorbed onto the samples for 1 h, followed by washing with PBS.

For cell attachment studies, the PBS was removed under sterile conditions, and the scaffolds were seeded with MG63 cells (20 000 cells cm^{-2}) with a total of 0.25 mL protein positive, or negative, growth media (protein positive: 87% DMEM, 10% FBS, 1% NEAA, 1% sodium pyruvate, 1% pen strep; protein negative: 97% DMEM, 1% NEAA, 1% sodium pyruvate, 1% pen strep). Empty wells were seeded with either protein positive, or negative, cell-containing media for controls. The samples were incubated (90 min, 37 °C, 5% CO_2) before fixation (3.7% formaldehyde, 15 min, room temperature (RT)). The samples were stained with 4′,6-diamidino-2-phenylindole, DAPI, (0.2 ng mL^{-1}, 5 min, RT) before being stored in PBS. Under low light levels, each sample was removed from its well and placed cell-side down on a glass microscope slide for viewing with an EVOS FL digital inverted microscope (objective: 10× Fl, excitation: 357 nm, emission: 447 nm). At least three images were acquired per sample repeat, and at least six repeat analyses were performed per sample. Triplicate tests were conducted using separate MG63 cell passages. The cell attachment on each hydrogel relative to the control (protein positive media, tissue culture treated plate) was determined by comparing the average number of cells imaged on each.

Statistics. IBM SPSS Statistics software was used for statistical analysis. For cell attachment and spreading studies, and hydrogel physiochemical properties, a one-way analysis of variance (ANOVA) test was used to determine the statistical differences between the means of two or more samples, assuming equal variance, with a Tukey posthoc comparison. The statistical differences between cell aspect ratio distributions were determined using the Kruskal−Wallis one-way ANOVA test. The differences were considered significant at the levels of $p < 0.001$, $p < 0.01$, and $p < 0.05$ with a confidence level of 0.95.

Regression Model. To ensure that the data were suitable for analysis, a normal probability plot for cell attachment was produced (Figure S4). The samples were ordered in increasing value and assigned an increasing corresponding number, one being assigned to the lowest value. The "z value", determined from the assigned number using the inverse of the standard normal cumulative distribution, was plotted against the sample standard deviation. If the line of best fit for the data set passed through (0,0) and had a high coefficient of determination, the model was deemed suitable for analysis.

Development of the regression model to predict cell attachment was performed using Excel with the solver add-in enabled. Constants were calculated using the solver function in Microsoft Excel using the GRG nonlinear solving method.[45] Both the sum of the differences between the model and real values, and the sum of the squared differences were minimized. For each potential model, a cross-validation (leave-one-out) methodology was employed: one result was omitted from the model before fitting. The coefficient of determination, R^2, was calculated from the six included results only, comparing the predicted value to the actual value, and the constants recorded. This was repeated six times further, suppressing each result in turn.[46] The average R^2 and constant values were calculated from the seven values generated. Two further coefficients of determination were calculated based on the averaged constant values: (i) Q^2 calculated from all of the seven results, comparing the predicted value to the actual value; and (ii) MV for the line of best fit for a plot of predicted values versus actual values for all of the seven results. To be designated as valid, the models had to meet four criteria: (i) $Q^2 > 0.5$; (ii) $R^2 - Q^2 < 0.2$; (iii) MV > 0.25; and (iv) the SE for each constant had to be less than the average constant value (Table S1).[47,48]

The optimal model was determined using four additional criteria to penalize the models: (i) $0.5/Q^2$; (ii) $(R^2 - Q^2)/0.2$; (iii) 0.25/MV; and (iv) (number of terms)/6. The model with the lowest sum from these criteria was chosen to be optimal (Table S2).

■ ASSOCIATED CONTENT

Supporting Information

The Supporting Information is available free of charge on the ACS Publications website at DOI: 10.1021/acsomega.7b01583.

Chitosan molecular weight determination, additional deconvoluted FTIR spectra, chitosan penetration depth data, cell morphology after 24 h characterization, normal probability plot for cell attachment, data for all of the valid cell models, and penalization data for all of the valid cell models (PDF)

■ AUTHOR INFORMATION

Corresponding Authors

*E-mail: j.l.scott@bath.ac.uk (J.L.S.).
*E-mail: r.sharma@bath.ac.uk (R.I.S.).

ORCID

Marcus A. Johns: 0000-0003-0176-8620
Evandro M. Lanzoni: 0000-0001-9784-0935
Paul M. Murray: 0000-0002-0277-5403
Janet L. Scott: 0000-0001-8021-2860
Ram I. Sharma: 0000-0003-3573-8403

DOI: 10.1021/acsomega.7b01583
ACS Omega 2018, 3, 937−945

Present Addresses

[¶]Department of Chemistry, Universidade Estadual de Campinas (UNICAMP), Campinas, SP 13083-970, Brazil (F.G.).

[⋈]Department of Aerospace Engineering, Queens Building, University Walk, Clifton, Bristol, BS8 1TR, UK (M.A.J.).

Author Contributions

The manuscript was written through contributions of all of the authors. All of the authors have given approval to the final version of the manuscript.

Notes

The authors declare no competing financial interest.

■ ACKNOWLEDGMENTS

The authors acknowledge the following funding: Ph.D. studentship funding for M.A.J. from the UK Engineering and Physical Sciences Research Council (EPSRC) via the EPSRC Doctoral Training Centre in Sustainable Chemical Technologies, University of Bath (EP/G03768X/1); and the British Council via the Global Innovation Initiative programme, which facilitated UK/Brazilian collaboration. Y.B. acknowledges the Paul Janmey laboratory for provision of the AFM analysis MATLAB scripts. All of the data are available from the University of Bath data archive at https://doi.org/10.15125/BATH-00400.

■ ABBREVIATIONS

ANOVA, one-way analysis of variance; DAPI, 4′,6-diamidino-2-phenylindole; d*C*/d*z*, capacitive coupling; DI, deionized water; DMEM, Dulbecco's modified Eagle's medium; DMSO, dimethyl sulfoxide; DoE, design of experiments; ECM, extracellular matrix; [EMIm][OAc], 1-ethyl-3-methylimidazolium acetate; FBS, fetal bovine serum; FITC, fluorescein phalloidin; FTIR, Fourier transform infrared; *G*, shear modulus; MeOH, methanol; NEAA, nonessential amino acids; OES, organic electrolyte solution; PBS, phosphate-buffered saline; pen strep, penicillin streptomycin; SIPN, semi-interpenetrating network; R_q, root mean square roughness; ζ, surface zeta potential

■ REFERENCES

(1) Yang, S.; Leong, K.-F.; Du, Z.; Chua, C.-K. The Design of Scaffolds for Use in Tissue Engineering. Part I. Traditional Factors. *Tissue Eng.* **2001**, *7*, 679−689.

(2) Webb, A. R.; Yang, J.; Ameer, G. A. Biodegradable polyester elastomers in tissue engineering. *Expert Opin. Biol. Ther.* **2004**, *4*, 801−812.

(3) McKee, C. T.; Last, J. A.; Russell, P.; Murphy, C. J. Indentation Versus Tensile Measurements of Young's Modulus for Soft Biological Tissues. *Tissue Eng., Part B* **2011**, *17*, 155−164.

(4) Frantz, C.; Stewart, K. M.; Weaver, V. M. The extracellular matrix at a glance. *J. Cell Sci.* **2010**, *123*, 4195−4200.

(5) Schaefer, L.; Schaefer, R. M. Proteoglycans: from structural compounds to signaling molecules. *Cell Tissue Res.* **2010**, *339*, 237−246.

(6) Majima, T.; Funakosi, T.; Iwasaki, N.; Yamane, S.-T.; Harada, K.; Nonaka, S.; Minami, A.; Nishimura, S.-I. Alginate and chitosan polyion complex hybrid fibers for scaffolds in ligament and tendon tissue engineering. *J. Orthop. Sci.* **2005**, *10*, 302−307.

(7) Francis, N. L.; Hunger, P. M.; Donius, A. E.; Riblett, B. W.; Zavaliangos, A.; Wegst, U. G. K.; Wheatley, M. A. An ice-templated, linearly aligned chitosan-alginate scaffold for neural tissue engineering. *J. Biomed. Mater. Res., Part A* **2013**, *101*, 3493−3503.

(8) Ceccaldi, C.; Bushkalova, R.; Alfarano, C.; Lairez, O.; Calise, D.; Bourin, P.; Frugier, C.; Rouzaud-Laborde, C.; Cussac, D.; Parini, A.; Sallerin, B.; Fullana, S. G. Evaluation of polyelectrolyte complex-based scaffolds for mesenchymal stem cell therapy in cardiac ischemia treatment. *Acta Biomater.* **2014**, *10*, 901−911.

(9) Augst, A. D.; Kong, H. J.; Mooney, D. J. Alginate Hydrogels as Biomaterials. *Macromol. Biosci.* **2006**, *6*, 623−633.

(10) Xiao, W.; Chen, Q.; Wu, Y.; Wu, T.; Dai, L. Dissolution and blending of chitosan using 1,3-dimethylimidazolium chloride and 1-H-3-methylimidazolium chloride binary ionic liquid solvent. *Carbohydr. Polym.* **2011**, *83*, 233−238.

(11) Stefanescu, C.; Daly, W. H.; Negulescu, I. I. Biocomposite films prepared from ionic liquid solutions of chitosan and cellulose. *Carbohydr. Polym.* **2012**, *87*, 435−443.

(12) Mututuvari, T. M.; Harkins, A. L.; Tran, C. D. Facile synthesis, characterization, and antimicrobial activity of cellulose−chitosan−hydroxyapatite composite material: A potential material for bone tissue engineering. *J. Biomed. Mater. Res., Part A* **2013**, *101*, 3266−3277.

(13) Liu, Z.; Huang, H. Preparation and characterization of cellulose composite hydrogels from tea residue and carbohydrate additives. *Carbohydr. Polym.* **2016**, *147*, 226−233.

(14) Schneider, G. B.; English, A.; Abraham, M.; Zaharias, R.; Stanford, C.; Keller, J. The effect of hydrogel charge density on cell attachment. *Biomaterials* **2004**, *25*, 3023−3028.

(15) Kim, S.; English, A. E.; Kihm, K. D. Surface elasticity and charge concentration-dependent endothelial cell attachment to copolymer polyelectrolyte hydrogel. *Acta Biomater.* **2009**, *5*, 144−151.

(16) Courtenay, J. C.; Johns, M. A.; Galembeck, F.; Deneke, C.; Lanzoni, E. M.; Costa, C. A.; Scott, J. L.; Sharma, R. I. Surface modified cellulose scaffolds for tissue engineering. *Cellulose* **2017**, *24*, 253−267.

(17) Engler, A. J.; Sen, S.; Sweeney, H. L.; Discher, D. E. Matrix Elasticity Directs Stem Cell Lineage Specification. *Cell* **2006**, *126*, 677−689.

(18) Sharma, R. I.; Snedeker, J. G. Biochemical and biomechanical gradients for directed bone marrow stromal cell differentiation toward tendon and bone. *Biomaterials* **2010**, *31*, 7695−7704.

(19) Lee-Thedieck, C.; Rauch, N.; Fiammengo, R.; Klein, G.; Spatz, J. P. Impact of substrate elasticity on human hematopoietic stem and progenitor cell adhesion and motility. *J. Cell Sci.* **2012**, *125*, 3765−3775.

(20) Diederich, V. E. G.; Studer, P.; Kern, A.; Lattuada, M.; Storti, G.; Sharma, R. I.; Snedeker, J. G.; Morbidelli, M. Bioactive polyacrylamide hydrogels with gradients in mechanical stiffness. *Biotechnol. Bioeng.* **2013**, *110*, 1508−1519.

(21) Lincks, J.; Boyan, B. D.; Blanchard, C. R.; Lohmann, C. H.; Liu, Y.; Cochran, D. L.; Dean, D. D.; Schwartz, Z. Response of MG63 osteoblast-like cells to titanium and titanium alloy is dependent on surface roughness and composition. *Biomaterials* **1998**, *19*, 2219−2232.

(22) Deligianni, D. D.; Katsala, N. D.; Koutsoukos, P. G.; Missirlis, Y. F. Effect of surface roughness of hydroxyapatite on human bone marrow cell adhesion, proliferation, differentiation and detachment strength. *Biomaterials* **2001**, *22*, 87−96.

(23) Thapa, A.; Webster, T. J.; Haberstroh, K. M. Polymers with nano-dimensional surface features enhance bladder smooth muscle cell adhesion. *J. Biomed. Mater. Res., Part A* **2003**, *67A*, 1374−1383.

(24) Martínez, E.; Engel, E.; Planell, J. A.; Samitier, J. Effects of artificial micro- and nano-structured surfaces on cell behaviour. *Ann. Anat.* **2009**, *191*, 126−135.

(25) Chang, H.-I.; Wang, Y. Cell Responses to Surface and Architecture of Tissue Engineering Scaffolds. In *Regenerative Medicine and Tissue Engineering - Cells and Biomaterials*; Eberli, D., Ed.; InTech: Rijeka, Croatia, 2011.

(26) Zhang, Z.; Cheng, X.; Yao, Y.; Luo, J.; Tang, Q.; Wu, H.; Lin, S.; Han, C.; Wei, Q.; Chen, L. Electrophoretic deposition of chitosan/gelatin coatings with controlled porous surface topography to enhance initial osteoblast adhesive responses. *J. Mater. Chem. B* **2016**, *4*, 7584−7595.

DOI: 10.1021/acsomega.7b01583
ACS Omega 2018, 3, 937−945

(27) Jung, J. P.; Moyano, J. V.; Collier, J. H. Multifactorial optimization of endothelial cell growth using modular synthetic extracellular matrices. *Integr. Biol.* **2011**, *3*, 185−196.
(28) Lam, J.; Carmichael, S. T.; Lowry, W. E.; Segura, T. Hydrogel Design of Experiments Methodology to Optimize Hydrogel for iPSC-NPC Culture. *Adv. Healthcare Mater.* **2015**, *4*, 534−539.
(29) Chen, W. L. K.; Likhitpanichkul, M.; Ho, A.; Simmons, C. A. Integration of statistical modeling and high-content microscopy to systematically investigate cell−substrate interactions. *Biomaterials* **2010**, *31*, 2489−2497.
(30) Rehmann, M. S.; Luna, J. I.; Maverakis, E.; Kloxin, A. M. Tuning microenvironment modulus and biochemical composition promotes human mesenchymal stem cell tenogenic differentiation. *J. Biomed. Mater. Res., Part A* **2016**, *104*, 1162−1174.
(31) Johns, M. A.; Bernardes, A.; De Azevedo, E. R.; Guimaraes, F. E. G.; Lowe, J. P.; Gale, E. M.; Polikarpov, I.; Scott, J. L.; Sharma, R. I. On the subtle tuneability of cellulose hydrogels: implications for binding of biomolecules demonstrated for CBM 1. *J. Mater. Chem. B* **2017**, *5*, 3879−3887.
(32) Alemán, J. V.; Chadwick, A. V.; He, J.; Hess, M.; Horie, K.; Jones, R. G.; Kratochvíl, P.; Meisel, I.; Mita, I.; Moad, G.; Penczek, S.; Stepto, R. F. T. Definitions of terms relating to the structure and processing of sols, gels, networks, and inorganic-organic hybrid materials (IUPAC Recommendations 2007). *Pure Appl. Chem.* **2007**, *79*, 1801−1829.
(33) Wang, Q. Z.; Chen, X. G.; Liu, N.; Wang, S. X.; Liu, C. S.; Meng, X. H.; Liu, C. G. Protonation constants of chitosan with different molecular weight and degree of deacetylation. *Carbohydr. Polym.* **2006**, *65*, 194−201.
(34) Xu, L.-C.; Siedlecki, C. A. Effects of surface wettability and contact time on protein adhesion to biomaterial surfaces. *Biomaterials* **2007**, *28*, 3273−3283.
(35) Tan, J. L.; Tien, J.; Pirone, D. M.; Gray, D. S.; Bhadriraju, K.; Chen, C. S. Cells lying on a bed of microneedles: An approach to isolate mechanical force. *Proc. Natl. Acad. Sci. U.S.A.* **2003**, *100*, 1484−1489.
(36) Courtenay, J. C.; Deneke, C.; Lanzoni, E. M.; Costa, C. A.; Bae, Y.; Scott, J. L.; Sharma, R. I. Modulating cell response on cellulose surfaces; tunable attachment and scaffold mechanics. *Cellulose* **2017**, DOI: 10.1007/s10570-017-1612-3.
(37) Wojdyr, M. Fityk: a general-purpose peak fitting program. *J. Appl. Crystallogr.* **2010**, *43*, 1126−1128.
(38) Tan, S. C.; Khor, E.; Tan, T. K.; Wong, S. M. The degree of deacetylation of chitosan: advocating the first derivative UV-spectrophotometry method of determination. *Talanta* **1998**, *45*, 713−719.
(39) Pöhlker, C.; Huffman, J. A.; Pöschl, U. Autofluorescence of atmospheric bioaerosols − fluorescent biomolecules and potential interferences. *Atmos. Meas. Tech.* **2012**, *5*, 37−71.
(40) Bae, Y. H.; Assoian, R. K.; VanHook, A. M. Science Signaling Podcast: 17 June 2014. *Sci. Signaling* **2014**, *7*, pc17.
(41) Bae, Y. H.; Liu, S.-l; Byfield, F. J.; Janmey, P. A.; Assoian, R. K. Measuring the Stiffness of Ex Vivo Mouse Aortas Using Atomic Force Microscopy. *J. Visualized Exp.* **2016**, *116*, No. e54630.
(42) Domke, J.; Radmacher, M. Measuring the Elastic Properties of Thin Polymer Films with the Atomic Force Microscope. *Langmuir* **1998**, *14*, 3320−3325.
(43) Ferreira, E. S.; Lanzoni, E. M.; Costa, C. A. R.; Deneke, C.; Bernardes, J. S.; Galembeck, F. Adhesive and Reinforcing Properties of Soluble Cellulose: A Repulpable Adhesive for Wet and Dry Cellulosic Substrates. *ACS Appl. Mater. Interfaces* **2015**, *7*, 18750−18758.
(44) Nečas, D.; Klapetek, P. Gwyddion: an open-source software for SPM data analysis. *Open Phys.* **2012**, *10*, 181−188.
(45) Lasdon, L. S.; Fox, R. L.; Ratner, M. W. Nonlinear optimization using the generalized reduced gradient method. *R.A.I.R.O. Rech. Oper.* **1974**, *8*, 73−103.
(46) Naes, T.; Isaksson, T.; Fearn, T.; Davies, T. *A User-friendly Guide to Multivariate Calibration and Classification*; NIR Publications: Chichester, U.K., 2002.
(47) Lundstedt, T.; Seifert, E.; Abramo, L.; Thelin, B.; Nyström, Å; Pettersen, J.; Bergman, R. Experimental design and optimization. *Chemom. Intell. Lab. Syst.* **1998**, *42*, 3−40.
(48) Eriksson, L.; Johansson, E.; Kettaneh-Wold, N.; Wikström, C.; Wold, S. *Design of Experiments: Principles and Applications*, 3rd ed.; Umetrics Academy: Umeå, Sweden, 2008.

DOI: 10.1021/acsomega.7b01583
ACS Omega 2018, 3, 937−945